ISSN 1974-9821
Vol. 5 N. 2
April 2012

International Review on Modelling and Simulations (IREMOS)

PART A

Contents:

(continued on inside back cover)

Praise Worthy Prize

International Review on Modelling and Simulations (IREMOS)

The ***International Review on Modelling and Simulations (IREMOS)*** is a publication of the **Praise Worthy Prize S.r.l..**
The Review is published bimonthly, appearing on the last day of February, April, June, August, October, December.

Published and Printed in Italy by **Praise Worthy Prize S.r.l.,** Naples, April 30, 2012.

Praise Worthy Prize

International Review on Modelling and Simulations (I.RE.MO.S.), Vol. 5, N. 2
ISSN 1974-9821 *April 2012*

Large-Scale Metamodeling and Validation of Power Systems

S. Shan, W. Zhang, G. G. Wang

Abstract – *Modeling the available transfer capacity of power systems is arduous due to contingencies and commonly performed by simulation. Meanwhile, both metamodeling and validating a large-scale computationally expensive simulation system is challenging due to "curse of dimensionality." This paper applies the recently developed Radial Basis Function-High Dimensional Model Representation (RBF-HDMR) to model the transfer capability of a 50-variable electric power system subject to contingency disturbances. The simulation-based transfer capability analysis has a combination of high-dimensional, computationally-expensive, and black-box features, which is called a HEB problem. The obtained RBF-HDMR is useful for power system analysis and operation planning. In addition, this work proposes two complementary sets of modified performance metrics for validation of metamodeling techniques in general. The proposed metrics overcome the deficiencies of some commonly-used metrics, and also the potential risk of using an individual or an arbitrary set of performance metrics, which is the common practice in the field of metamodeling.*

The accuracy and efficiency of RBF-HDMR, as well as the application of the two sets of performance metrics, are demonstrated through three practical cases under different operating scenarios for the given power system. The results show that RBF-HDMR is effective and efficient in modeling this large-scale HEB problem, and moreover, the two sets of performance metrics overcome the potential misjudgment might have been brought by using individual metrics.

Keywords: *Power System Modeling, Power Generation Economics, Power System Interconnection, Power System Planning, Large-scale Systems, Power System Simulation, Metamodeling*

Nomenclature

HDMR	High dimensional model representation
HEB	A combination of high-dimensional, computationally-expensive, and black-box features
IPLAN	A programming language
$MARE$	Mean absolute relative error
$MdARE$	Median absolute relative error
MSE	Mean square error
$MxARE$	Maximum absolute relative error
MW	Mega watts
OMT	Ontario-manitoba tie
OPF	Optimal power flow
PSS/E	Power System Simulator for Engineering
RAAE	Relative average absolute error
RBF	Radial basis function
RBF-HDMR	Radial basis function-high dimensional model representation
$RMAE$	Relative maximum absolute error
R Square	Metric to test metamodel
$SM_{d\times n}$	$d \times n$ structure matrix
STD	Standard deviation
SVR	Support vector regression
V	Variance
$\|\cdot\|$	P-norm distance
$\phi(\cdot)$	Radial basis function
α	Coefficient vector
α_{i_k}, α_{ij_k}, …	Coefficients of the expression
$\boldsymbol{\beta}$	Coefficient vector
ε	Approximation error
"0"	Variable does not appear in the component term
"1"	Variable appears in the component term
2^d	Number of component terms
$\boldsymbol{A}$	Distance matrix
A_{ij}	Element in distance matrix
d	Number of dimensionality
e_i	Relative error
f_0	Constant term evaluated at $\boldsymbol{x}_0$
$\bar{f}$	Mean of function
$f(\boldsymbol{x})$	Output function
$\hat{f}(\boldsymbol{x})$	Approximation of $f(\boldsymbol{x})$
$f_{12\ldots d}$	D-variate correlation component term
L_1	Absolute value of the piecewise difference between the actual value $f(\boldsymbol{x_i})$ and predicated value $\hat{f}(\boldsymbol{x_i})$

Manuscript received and revised March 2012, accepted April 2012

L_2	Square root of the piecewise square of the difference between the actual value $f(\boldsymbol{x_i})$ and predicted value $\hat{f}(\boldsymbol{x_i})$
$m_i, m_{ij}, \ldots,$	Number of sampled points for each term
n	Number of component terms
$P(\boldsymbol{x})$	Polynomial function
$\tilde{P}_{ij}$	Implementation of polynomial function
$\boldsymbol{x}_0$	Chosen reference point
$\boldsymbol{x}_0^i, \boldsymbol{x}_0^{ij}$	$\boldsymbol{x}_0$ without element/s x_i, x_i and x_j
$(x_{i_k}, \boldsymbol{x}_0^i)$, $(x_{i_k}, x_{j_k}, \boldsymbol{x}_0^{ij})$	Sampled points of input variables or the centers of radial basis function

I. Introduction

Metamodeling [1] provides an effective mechanism for facilitating simulation processes and simplifying the interpretation of simulation results. These techniques construct a mathematical model of simulation analysis by a well-planned sampling scheme to relate the simulation outputs as a function of relevant input factors. The mathematical model of this kind is called a metamodel, since it is a model of the simulation model. The planned sampling is also known as the design of computer experiments. After validation, the metamodel often surrogates the expensive simulation processes for system analysis and optimization.

There are various metamodels developed and studied, for example, polynomial response surface [1],[2], Kriging model [3],[4], radial basis function (RBF) [5],[6], and support vector regression (SVR) [7]. These models are often selected based on practitioners' experience or knowledge. The choice of a model type affects metamodeling results. The works [5], [7], [8] compared the performance of some of these metamodels. With advances in metamodeling techniques and increase in demands for application, some researchers attempt to exploit the best one of multiple fitting metamodels based on certain criteria or constructing a weighed metamodel consisting of multiple individual models to increase metamodels' accuracy and capabilities (see [9]-[11]).

Metamodeling techniques have been widely used in various disciplines. In mechanical engineering, Kuczera and Mourelatos [12] solved the reliability analysis of multiple failure region problems by the use of metamodels as indicators to determine the failure and safe regions. Yang *et al.* [13] used five metamodeling techniques for vehicle frontal impact simulation. Apley *et al.* [14] applied metamodeling techniques to an engine piston design problem and studied the effort of modeling uncertainty in robust design. In electrical engineering, Georgopoulou and Giannakoglou [15] proposed a metamodel-assisted evolutionary algorithm to solve power generating unit commitment with probabilistic outages. Shan *et al.* [16] successfully applied the metamodeling methodologies to the transfer capability of a power grid with five input variables. AL-Masri *et al.* [17] use artificial neural network to assess the power system security. Kaewarsa and Attakitmongcol [18] classify power quality disturbances by support vector machines.

From both foundational development and applications of metamodeling techniques, a general impression is that most of these successful cases are low-dimensional problems. HEB (a combination of high-dimensional, computationally-expensive, and black-box features) problems are challenging for metamodels and sampling methods. Computational complexity for HEB problems arises with the increase in dimensionality, known as "curse of dimensionality." For example, for a problem with 50 variables, if a two-level-per-factor design of computer experiments is taken, 2^{50} simulations are needed. If each simulation needs 13 minutes to run (as is the case for the Manitoba power system in this work), it needs 2.8234×10^{10} years to implement in total. Obviously, the computation expense is formidable for high-dimensional cases. Shan and Wang [19] reviewed the strategies to solve HEB problems. The existing techniques are often limited in their respective ways. For example, dimensionality reduction techniques are not applicable for problems in which each variable has similar importance. Recently a novel RBF-HDMR [20],[21] has been developed based on HDMR theories [22],[23]. This work uses the RBF-HDMR to model the transfer capability analysis of a large-scale power system.

In the aspect of metamodel validation, there are a collection of papers addressing performance metrics and methodology (for instance, [24], [25]). The validation depends on the purpose of metamodeling [26]. Different purposes lead to various validation performance metrics and approaches. For example, Kleijnen and Sargent [26] prefer the absolute error than the absolute relative error, if a single large error is catastrophic (for example, in nuclear simulations), the maximum error will be an important performance metric. Different validation performance metrics have their pros and cons [27]. Numerous performance metrics have been listed in literature [19]. However, individual performance metrics, if used alone, are often unable to completely reflect the accuracy and/or effectiveness of metamodeling, which misleads the modeler. This is because the characteristics of original systems are unknown prior to metamodeling and individual or any arbitrary set of performance metrics have limitations in certain situations, which will be elaborated later in this work. To overcome such limitations, this paper proposes two complementary sets of modified performance metrics for validation of metamodeling techniques in general.

In this work, the metamodeling and application of the performance metrics for validation are demonstrated through the application in modeling power systems. Modeling the available transfer capability of power systems is challenging [28]. Power system analysis is crucial for reliable and efficient operations, which is commonly performed by simulation. This work models the power transfer capability at the Manitoba-Ontario interconnection, which is defined as the maximum power

that can be sold from Manitoba to Ontario subject to system contingency requirements. The control parameters are outputs from 50 generators located in six hydraulic generating plants along the Winnipeg River and a thermal generating plant at Selkirk, a suburb of Winnipeg. Currently there lacks of a formal approach to determine the maximum transfer capability. Engineers have to assume a generation pattern and then evaluate the pattern through intensive simulation.

This approach has three major drawbacks: 1) it is impossible to exhaust all the possible generation patterns, 2) time-consuming, and 3) lack of understanding of the underlying power system, in specific, the relationship between the generator outputs and the power transfer capability while satisfying all of the contingency and reliability constraints.

This work applies the RBF-HDMR to capture the relationship between the 50 generator outputs and the maximum power transfer capability. The model is validated against the proposed two sets of metrics, as well as by field experts.

The work is organized as follows. Section 2 describes the framework of the methodology. Section 3 introduces RBF-HDMR and its sampling scheme. Section 4 proposes two complementary sets of modified performance metrics for metamodel validation. Section 5 presents case studies. Summary is given in Section 6.

II. Framework of Methodology

As introduced, this study employs RBF-HDMR to build a mathematical model of the maximized transfer capability of interconnected power system on the Manitoba-Ontario interconnection. In specific, the process starts with systematically planned sampling of generation patterns; a generation pattern is defined as the vector of all power outputs from the generators. The generation patterns are inputs to the power system simulation model, on which various analyses and contingency checks are performed.

The simulation output is the feasibility of the sample point (generation pattern) and the maximum power that can be transferred for a given input without causing system instability under various contingency conditions. Once the samples have been evaluated, a metamodel can be built for the transfer capability as a function of the generation patterns.

After validation, the metamodel can be used to plan the interchange across the interconnections under forecast system operating conditions. Fig. 1 delineates the framework of the methodology.

In the procedures of Fig. 1, loading model represents starting the simulation model under a specified operating condition; sampling is to simulate the inputs, that is, the generation patterns; contingency analyses for the given input are performed by the power system simulation tool PSS/E™ (Power System Simulator for Engineering). An in-house IPLAN (a programming language designed to be utilized as an enhancement to existing application programs such as PSS/E) [29] program is run to search for the corresponding maximum transferrable power, which is modeled as the power transfer capability by RBF-HDMR. In specific, for a given generation pattern, the output (the maximum transfer capability) is obtained by iteratively setting a transfer level, running PSS/E contingency analysis for all defined area contingencies, and checking the system responses against all the reliability criteria.

If all checks are passed, the transfer level is incremented and the process is repeated until a limit is found.

This transfer limit is then used as the output (a sample to the metamodeling process). The RBF-HDMR treats power system simulation and the search for the maximum transferrable power in the dash box as a black-box function, that is, it uses the input/output data without the knowledge about how the simulation model processes these inputs to get outputs.

After validation, the RBF-HDMR modeling process is completed and the resultant RBF-HDMR model can be used for system planning.

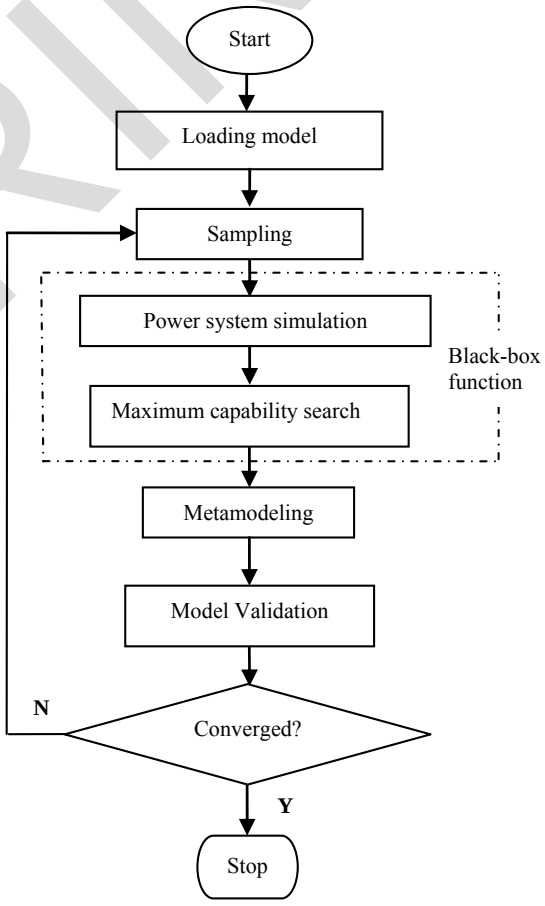

Fig. 1. Framework of the methodology

It is to be noted that the metamodel is not built on steady-state fixed situations; it considers numerous contingencies and system reliability constraints. In other words, the metamodel is the model captures the

generation pattern and the maximum possible transfer limit when all of the contingencies and system constraints are satisfied.

This problem differs from the traditional optimal power flow (OPF) problem and cannot be solved by OPF tools.

III. RBF-HDMR Techniques

III.1. RBF-HDMR Model

A general RBF-HDMR model [20] is written as:

$$f(\boldsymbol{x}) \cong f_0 + \sum_{i=1}^{d}\sum_{k=1}^{m_i} \alpha_{i_k}\left|\left(x_i, \boldsymbol{x}_0^i\right) - \left(x_{i_k}, \boldsymbol{x}_0^i\right)\right| + \\ + \sum_{1\le i<j\le d}\sum_{k=1}^{m_{ij}} \alpha_{ij_k}\left|(x_i, x_j, \boldsymbol{x}_0^{ij}) - (x_{i_k}, x_{j_k}, \boldsymbol{x}_0^{ij})\right| + \\ + \sum_{k=1}^{m_{12\cdots d}} \alpha_{12\cdots d_k}|\boldsymbol{x} - \boldsymbol{x}_k| \quad (1)$$

where f_0 denotes the constant term evaluated at $\boldsymbol{x}_0$ (any chosen reference point in modeling domain); $\boldsymbol{x}_0^i$, $\boldsymbol{x}_0^{ij}$, …, are respectively $\boldsymbol{x}_0$ without element/s x_i, x_i and x_j, …, (that is, $\left(x_i, \boldsymbol{x}_0^i\right) = \left[x_{1_0}, x_{2_0}, \cdots, x_{i-1_0}, x_i, x_{i+1_0}, \cdots, x_{d_0}\right]^T$, $(x_i, x_j, \boldsymbol{x}_0^{ij}) = \begin{matrix}[x_{1_0}, x_{2_0}, \cdots, x_{i-1_0}, x_i, x_{i+1_0}, \\ \cdots x_{j-1_0}, x_j, x_{j+1_0}, \cdots, x_{d_0}]\end{matrix}^T$, respectively represents a point in the modeling domain); d is the number of dimensionality for the input variable vector $\boldsymbol{x}$; $|.|$ denotes a p-norm distance; α_{i_k}, α_{ij_k}, …, $\alpha_{12\cdots d_k}$ are respectively the coefficient of the expression and $(x_{i_k}, \boldsymbol{x}_0^i)$, $(x_{i_k}, x_{j_k}, \boldsymbol{x}_0^{ij})$, …, $\boldsymbol{x}_k$ are the sampled points of input variables or the centers of radial basis function (RBF) approximation; m_i, m_{ij}, …, $m_{12\cdots d}$ are the number of sampled points for each term; the component $\sum_{k=1}^{m_i} \alpha_{i_k}\left|\left(x_i, \boldsymbol{x}_0^i\right) - \left(x_{i_k}, \boldsymbol{x}_0^i\right)\right|$ represents the ith input variable x_i term which explains the effect of the ith input variable x_i independently acting on the output function $f(\boldsymbol{x})$; the component $\sum_{k=1}^{m_{ij}} \alpha_{ij_k}\left|(x_i, x_j, \boldsymbol{x}_0^{ij}) - (x_{i_k}, x_{j_k}, \boldsymbol{x}_0^{ij})\right|$ denotes the correlated contribution of the variables x_i and x_j upon the output $f(\boldsymbol{x})$ after the individual influences of x_i and x_j are discounted; the subsequent similar components reflect the effects of increasing numbers of correlated variables acting together upon the output $f(\boldsymbol{x})$.

The last component $\sum_{k=1}^{m_{12\cdots d}} \alpha_{12\cdots d_k}|\boldsymbol{x} - \boldsymbol{x}_k|$ models any residual dependence of all the variables locked together to influence the output $f(\boldsymbol{x})$ after all the lower-order correlations and individual influence of each involved x_i (i =1,…,d) have been discounted.

Without losing generality, the model (1) uses a simple linear spline function as the basis function for the ease of description and understanding; in implementation, a sum of thin plate spline plus a linear polynomial given in Appendix is used to avoid singular matrices.

The functional form of the RBF-HDMR is represented by its structure matrix which is defined as:

$$SM_{d\times n} = \begin{bmatrix} 0\,1\,0\,0\,\ldots\,0\,1\,\ldots\,0\,\ldots\,0\,\ldots\,1 \\ 0\,0\,1\,0\,\ldots\,0\,1\,\ldots\,0\,\ldots\,0\,\ldots\,1 \\ 0\,0\,0\,1\,\ldots\,0\,0\,\ldots\,0\,\ldots\,0\,\ldots\,1 \\ \ldots \\ 0\,0\,0\,0\,\ldots\,0\,0\,\ldots\,0\,\ldots\,1\,\ldots\,1 \\ 0\,0\,0\,0\,\ldots\,1\,0\,\ldots\,0\,\ldots\,1\,\ldots\,1 \end{bmatrix} \quad (2)$$

where d is the dimensionality of the input variable vector $\boldsymbol{x}$; n denotes the number of to-be-decided component terms of the model (1). Each row corresponds to a variable x_i. Each column corresponds to one of the component terms in (1). Each element in the structure matrix is assigned as "0" or "1" ; "0" means that the variable does not appear in the component term; "1" means that the variable appears in the component term. For example, the column $[0_1, 0_2, \ldots, 0_d]^T$ denotes the constant component term f_0; $[0_1, 0_2, \ldots, 0_{i-1}, 1_i, 0_{i+1}, \ldots, 0_d]^T$ represents the first-order component term $f_i(x_i)$; $[0_1, 0_2, \ldots, 0_{i-1}, 1_i, 0_{i+1}, \ldots, 0_{j-1}, 1_j, 0_{j+1}, \ldots, 0_d]^T$ indicates the existence of the second-order component term $f_{ij}(x_i, x_j)$, and the last column indicates the existence of d-variate correlation component term $f_{12\ldots d}(x_1, x_2, \ldots, x_d)$. In total, there are 2^d number of component terms; however, many components may not exist and some others disappear due to their negligible contribution to $f(\boldsymbol{x})$. The structure matrix is gradually generated with the RBF-HDMR modeling process. It uniquely indexes the component terms and explicitly expresses the functional form of black-box functions [20], [21].

The RBF-HDMR has many attractive features: 1) it has an explicit functional form to "reveal" correlation among the variables; 2) it provides with (non)linearity information with regard to inputs; 3) it discloses relative importance of variable terms, and 4) it efficiently and effectively models large scale complex systems (for example, high-dimensional nonlinear problems) [20],[21].

III.2. Sampling and Metamodeling Scheme

The sampling scheme of RBF-HDMR is an augmentative and adaptive process. The augmentation is carried out sequentially from the lower to higher orders, namely 0D, 1D, 2D, 3D, …, illustrated by Figs 2(a)-(d) and new samples are gradually added . The adaptive sampling is performed according to the linearity (or accuracy if nonlinearity appears) of the underlying function, and whether or no new terms exist in the function. In Figs. 2, the dots denote new sampling points.

The circles denote the sampling points inherited from previous order/s. The inherited sampling points in Fig. 2(d) are ignored for clarity. Those circles are distributed

on orthogonal axes or planes passing the reference points (the center point), as shown in both Figs. 2(b) and 2(c).

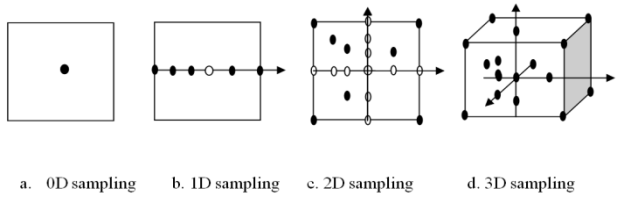

Figs. 2 An illustration of RBF-HDMR sampling scheme up to the 3rd order

Starting from the second-order (2D), new sampling points are not on those axes (≥2D) or planes (≥3D). As seen from Figs. 2(c) and 2(d), the sampling points are augmented with corner points first, then points close to center points of each quadrant, if needed, and at last other areas that need more exploration according to the characteristics of the underlying function. More detailed sampling steps are described as follows:

1. Choose a reference point $\boldsymbol{x}_0 = [x_{1_0}, x_{2_0}, \cdots, x_{d_0}]^T$ in the modeling domain (see Fig. 2(a)). It is recommended that taking the point $\boldsymbol{x}_0$ makes $f_0 = \bar{f}$ (that is, the mean of the function $f(\boldsymbol{x})$ in the modeling domain). Due to unknown mean of the function, this work takes one point in the neighborhood of the center of the modeling domain. Evaluating $f(\boldsymbol{x})$ at $\boldsymbol{x}_0$, we then have f_0. According to the theory of HDMR and the premise, the reference $\boldsymbol{x}_0$ is irrelevant if the model converges.

2. Sample for the first-order component functions $\sum_{k=1}^{m_i} \alpha_{i_k} \left| (x_i, \boldsymbol{x}_0^i) - (x_{i_k}, \boldsymbol{x}_0^i) \right| = f\left([x_{1_0}, x_{2_0}, \cdots, x_{i-1_0}, x_i, x_{i+1_0}, \cdots, x_{d_0}]^T\right) - f_0$ in the close neighborhood of the two ends of x_i direction (lower and upper limits) while fixing the rest of x_j ($j \neq i$) components at $\boldsymbol{x}_0$. In this work, a neighborhood is defined as one percent of the variable range which is in the design space and near a designated point. Evaluating these two end points, we got the left point value:

$$\alpha_{i_L} \left| (x_i, \boldsymbol{x}_0^i) - (x_{i_L}, \boldsymbol{x}_0^i) \right| = = f\left([x_{1_0}, x_{2_0}, \cdots, x_{i-1_0}, x_{i_L}, x_{i+1_0}, \cdots, x_{d_0}]^T\right) - f_0$$

and the right point value:

$$\alpha_{i_R} \left| (x_i, \boldsymbol{x}_0^i) - (x_{i_R}, \boldsymbol{x}_0^i) \right| = = f\left([x_{1_0}, x_{2_0}, \cdots, x_{i-1_0}, x_{i_R}, x_{i+1_0}, \cdots, x_{d_0}]^T\right) - f_0$$

and define the component function as $\sum_{k=1}^{m_i} \alpha_{i_k} \left| (x_i, \boldsymbol{x}_0^i) - (x_{i_k}, \boldsymbol{x}_0^i) \right|$ by finding coefficients α_{i_L}, α_{i_R}, … for each variable x_i (see Fig. 2(b)).

3. Check the linearity of $\sum_{k=1}^{m_i} \alpha_{i_k} \left| (x_i, \boldsymbol{x}_0^i) - (x_{i_k}, \boldsymbol{x}_0^i) \right|$. If the approximation model $\sum_{k=1}^{m_i} \alpha_{i_k} \left| (x_i, \boldsymbol{x}_0^i) - (x_{i_k}, \boldsymbol{x}_0^i) \right|$ built in the previous Step 2 goes through the center point, $\boldsymbol{x}_0$ (that is, $x_i = x_{i_0}$), $\sum_{k=1}^{m_i} \alpha_{i_k} \left| (x_i, \boldsymbol{x}_0^i) - (x_{i_k}, \boldsymbol{x}_0^i) \right|$ is considered as linear. In this case, modeling for this component terminates; otherwise, use the center point $\boldsymbol{x}_0$ to update $\sum_{k=1}^{m_i} \alpha_{i_k} \left| (x_i, \boldsymbol{x}_0^i) - (x_{i_k}, \boldsymbol{x}_0^i) \right|$. Then a random value along x_i is generated and combined with the rest of x_j ($j \neq i$) components at $\boldsymbol{x}_0$ to form a new point to test $\sum_{k=1}^{m_i} \alpha_{i_k} \left| (x_i, \boldsymbol{x}_0^i) - (x_{i_k}, \boldsymbol{x}_0^i) \right|$. If $\sum_{k=1}^{m_i} \alpha_{i_k} \left| (x_i, \boldsymbol{x}_0^i) - (x_{i_k}, \boldsymbol{x}_0^i) \right|$ is not sufficiently accurate (the relative prediction error is larger than a given criterion, for instance, 0.01%), the test point and all the evaluated points will be used to re-construct $\sum_{k=1}^{m_i} \alpha_{i_k} \left| (x_i, \boldsymbol{x}_0^i) - (x_{i_k}, \boldsymbol{x}_0^i) \right|$.

This sampling-remodeling process iterates until convergence. This process is to capture the nonlinearity of the component function with one sample point at a time. Step 3 repeats for all of the first-order component functions to construct the first-order terms of RBF-HDMR model individually (see Fig. 2b).

4. Form a new point:

$$(x_1, x_2, \cdots x_d)_k = \begin{bmatrix} x_{1_k}, x_{2_k}, \cdots, x_{i-1_k}, x_{i_k}, x_{i+1_k}, \cdots, \\ x_{j-1_k}, x_{j_k}, x_{j+1_k}, \cdots, x_{d_k} \end{bmatrix}^T, \quad k \neq 0$$

by randomly combining the sampled value x_i in the first-order component construction for each input variable (that is, x_i, $i = 1,...,d$ and evaluated at $(x_i, \boldsymbol{x}_0^i)$, respectively). This new point is then evaluated by expensive simulation and the first-order RBF-HDMR model.

The values of expensive simulation and model prediction are compared. If the two values are sufficiently close (the relative error is less than a small value, for example, 0.01%), it indicates that no higher order terms exist in the underlying function, the modeling process terminates. Otherwise, go to the next step.

This new point does not appear in Fig. 2 since it has high dimensionality.

5. Use the values of x_i and x_j, $i \neq j$ that exist in thus-far evaluated points:

$$(x_i, \boldsymbol{x}_0^i) = [x_{1_0}, x_{2_0}, \cdots, x_{i-1_0}, x_i, x_{i+1_0}, \cdots, x_{d_0}]^T$$

and:

$$(x_j, \boldsymbol{x}_0^j) = [x_{1_0}, x_{2_0}, \cdots, x_{j-1_0}, x_j, x_{j+1_0}, \cdots, x_{d_0}]^T$$

to form new points of the form:

$$(x_i, x_j, \boldsymbol{x}_0^{ij}) = \begin{matrix} [x_{1_0}, x_{2_0}, \cdots, x_{i-1_0}, x_i, x_{i+1_0}, \\ \cdots, x_{j-1_0}, x_j, x_{j+1_0}, \cdots, x_{d_0}]^T \end{matrix}$$

Randomly select one of the points from these new points (for example, one of four corners) to test the first-order RBF-HDMR model.

The corner points on x_i and x_j planes (see Fig. 2(c)) have high priority.

If the model passes through the new point, it indicates that x_i and x_j are not correlated and the process continues with the next pair of input variables.

This is to save the cost of modeling non-existing or insignificant correlations; otherwise, use this new point and the evaluated points $(x_i, \boldsymbol{x}_0^i)$ and $(x_j, \boldsymbol{x}_0^j)$ to construct the second-order component function, $\sum_{k=1}^{m_{ij}} \alpha_{ij_k} \left| (x_i, x_j, \boldsymbol{x}_0^{ij}) - (x_{i_k}, x_{j_k}, \boldsymbol{x}_0^{ij}) \right|$.

This sampling-remodeling process iterates for all possible two-variable correlations until convergence (the relative prediction error is less than 0.01%). Step 5 is repeated for all pairs of input variables.

Step 5 applies to all higher-order terms in RBF-HDMR model in a similar manner, which is shown in Fig. 2(d). Ref. [21] described in detail how further computation savings are achieved by employing derived theorems for higher-order terms.

IV. Model Validation

Metamodels need to be validated prior to use. The validation naturally involves performance metrics. Whatever performance metrics are used, the judgment of goodness of a metamodel is related to the nature of the underlying system and application requirements of the metamodel.

The intrinsic characteristics of real-world systems may lead to poor performance metrics. For example, a constant function causes that relative performance metrics divided by zeros, which leads to a high relative metric value and thus the conclusion of a poor metamodel. Some application requires that maximum error not exceed a limit, while others need the global metamodel has minimum total errors. Single performance metric reflects one aspect of a metamodel and none of a single performance is the best criterion for all circumstances.

Moreover, due to diversity of underlying systems' features and lack of *a priori* knowledge about these diversities, one performance metric or even one class of similar performance metrics may not be able to reflect the goodness of metamodels.

This work introduces two complementary sets of performance metrics: function-value-scaled and function-variability-scaled groups.

The goodness of a metamodel approximating an unknown function is commonly measured by some distance. The distance measure includes L_1 distance and L_2 distance. L_1 distance is the absolute value of the piecewise difference between the actual value $f(\boldsymbol{x_i})$ and predicated value $\hat{f}(\boldsymbol{x_i})$; while L_2 distance provides the square root of the piecewise square of the difference between the actual value $f(\boldsymbol{x_i})$ and predicted value $\hat{f}(\boldsymbol{x_i})$.

Whether the distance is scaled or mathematically changed further leads to different expressions to form various performance metrics.

The scaled performance metrics are often used to eliminate the influence of variations in function units and scales. In this work, the proposed function-value-scaled group is relatively scaled to the values of functions (based on L_1 distance), and the function-variability-scaled group is relatively scaled to the variability of functions (for instance, deviations or variations of functions, based on L_2 distance).

IV.1. Function-Value-Scaled Set

This group of performance metrics addresses the goodness of approximation models with regard to the values of the underlying function.

1) Mean Absolute Relative Error (MARE) percentage with *m* sample points, a mean absolute relative error percentage is defined as:

$$MARE = \frac{100}{m} \sum_{i=1}^{m} e_i,$$

$$e_i = \begin{cases} \left| \dfrac{f(\boldsymbol{x}_i) - \hat{f}(\boldsymbol{x}_i)}{f(\boldsymbol{x}_i)} \right|, & |f(x_i)| \geq 1 \\ \min \left(\left| \dfrac{f(\boldsymbol{x}_i) - \hat{f}(\boldsymbol{x}_i)}{f(\boldsymbol{x}_i)} \right|, \dfrac{|f(\boldsymbol{x}_i) - \hat{f}(\boldsymbol{x}_i)|}{(|f(\boldsymbol{x}_i)| + |\hat{f}(\boldsymbol{x}_i)|)/2} \right) & |f(x_i)| < 1 \end{cases} \quad (3)$$

$$i = 1, \cdots, m.$$

The relative error e_i piecewise measures the error of the model.

Note that the relative error $e_i = \left| \frac{f(x_i) - \hat{f}(x_i)}{f(x_i)} \right|$ is inflated when function values approach or equal to zero. Such inflation is alleviated by taking the minimum of $e_i = \left| \frac{f(x_i) - \hat{f}(x_i)}{f(x_i)} \right|$ and $e_i = \frac{|f(x_i) - \hat{f}(x_i)|}{(|f(x_i)| + |\hat{f}(x_i)|)/2}$.

2) Maximum Absolute Relative Error (MxARE) percentage a maximum absolute relative error percentage is defined as:

$$MxARE = \\ = 100 * max \left(\left| \frac{f(\boldsymbol{x}_1) - \hat{f}(\boldsymbol{x}_1)}{f(\boldsymbol{x}_1)} \right|, \left| \frac{f(\boldsymbol{x}_2) - \hat{f}(\boldsymbol{x}_2)}{f(\boldsymbol{x}_2)} \right|, \cdots, \left| \frac{f(\boldsymbol{x}_m) - \hat{f}(\boldsymbol{x}_m)}{f(\boldsymbol{x}_m)} \right| \right) \quad (4)$$

The absolute relative error percentage definition is to expose the behavior of the underlying system in extreme cases.

MARE and MxARE complement each other within this set of performance metrics, as one describes the

average and the other the maximum relative error, respectively.

3) Median Absolute Relative Error (MdARE) percentage"Median" in median absolute relative error (MdARE) percentage is defined as:

$$MdARE = 100 * median\left(\begin{array}{c} \left|\frac{f(\boldsymbol{x}_1) - \hat{f}(\boldsymbol{x}_1)}{f(\boldsymbol{x}_1)}\right|, \\ \left|\frac{f(\boldsymbol{x}_2) - \hat{f}(\boldsymbol{x}_2)}{f(\boldsymbol{x}_2)}\right|, \\ \ldots, \left|\frac{f(\boldsymbol{x}_m) - \hat{f}(\boldsymbol{x}_m)}{f(\boldsymbol{x}_m)}\right| \end{array} \right) \quad (5)$$

In this set of performance metrics, MARE is a global performance metric. In general, the smaller is the value of MARE, the better is the metamodel; $MxARE$ is a local performance metric, which not only reflects the status of one sample point, but also signals whether inflation appears in MARE in the vicinity whereas $f(\boldsymbol{x}_m)$ approaches zero. If an inflation appears in $MARE$, practitioners shall acknowledge it and modify the application of MARE around the zero-value area. MdARE assists MARE and $MxARE$ to measure a metamodel by providing the median value of the relative error.

IV.2. Function-Variability-Scaled Set

The second group of performance metrics deals with the goodness of approximation models with regard to the variability of underlying systems:

1) R Square

The error of a function $f(\boldsymbol{x})$ being approximated by $\hat{f}(\boldsymbol{x})$ can be estimated by the normalized Euclidean distance as:

$$\varepsilon = \frac{1}{V}\int \left[f(\boldsymbol{x}) - \hat{f}(\boldsymbol{x})\right]^2 d\boldsymbol{x} \quad (6)$$

where V denotes the variance of $f(\boldsymbol{x})$. If m sample points are taken and the function is square integrable:

$$\varepsilon = \frac{1}{Vm}\sum_{i=1}^{m}\left[f(\boldsymbol{x_i}) - \hat{f}(x_i)\right]^2 = \frac{MSE}{V} \quad (7)$$

The variance V describes the irregularities of the actual system and is independent from the approximation. MSE is the mean square error capturing the departure of the approximation model from the real system. In general, the smaller is the value of ε, the better is the approximation. However, this metric depends on the variance V, the intrinsic variability feature of $(\boldsymbol{x})$. In order to explain the drawback of using ε as a validation metric, according to the definition of variance, we rewrite:

$$\varepsilon = \frac{\sum_{i=1}^{m}\left[f(\boldsymbol{x_i}) - \hat{f}(x_i)\right]^2}{\sum_{i=1}^{m}\left[f(\boldsymbol{x_i}) - \bar{f}(\boldsymbol{x})\right]^2} \quad (8)$$

where $\bar{f}(\boldsymbol{x})$ is the mean of the function $f(\boldsymbol{x})$ in the defined domain. As one can see, the error ε becomes inflated while the function output is or close to be a constant.

The goodness of modeling is often estimated by R Square, which is defined as [5]:

$$R^2 = 1 - \frac{\sum_{i=1}^{m}[f(\boldsymbol{x}_i) - \hat{f}(\boldsymbol{x}_i)]^2}{\sum_{i=1}^{m}[f(\boldsymbol{x}_i) - \bar{f}(\boldsymbol{x}_i)]^2} \quad (9)$$

obviously:

$$R^2 = 1 - \varepsilon \quad (9')$$

Normally, if an approximation has $\varepsilon \ll 1$ or R square approaches one, then this approximation is believed to have a good accuracy with regard to variability. Similar to MARE, R square is deficient when V is close to zero. Let us assume that $f(\boldsymbol{x})$ in the defined domain is or close to a constant, that is, the mean of $f(\boldsymbol{x})$, and when $\hat{f}(\boldsymbol{x_i})$ closely approaches $f(\boldsymbol{x_i})$ (therefore, a good approximation), we have:

$$\varepsilon = lim_{\substack{f(\boldsymbol{x})\to\bar{f}(\boldsymbol{x}) \\ f(\boldsymbol{x_i})\to f(\boldsymbol{x_i})}} \frac{\sum_{i=1}^{m}\left[f(\boldsymbol{x_i}) - \hat{f}(\boldsymbol{x_i})\right]^2}{\sum_{i=1}^{m}\left[f(\boldsymbol{x_i}) - \bar{f}(\boldsymbol{x})\right]^2} = 1 \quad (10)$$

and then R square approaches zero.

In RBF-HDMR expressed in (1), the roughest approximation is the 0th order approximation $f(\boldsymbol{x}) \cong f_0$.

Then, the best 0th order approximation is $f_0 = \bar{f}$. Assuming the output $f(\boldsymbol{x})$ is a constant, $f(\boldsymbol{x}) \equiv f_0 \equiv \bar{f}$ indicates that the $\hat{f} = f_0$ accurately models $f(\boldsymbol{x})$ and there is no need for higher-order terms.

This corresponds to the scenario of $\varepsilon = 1$ or R square is 0. Hence if $\varepsilon \cong 1$ or R Square approaches zero, one cannot conclude that the approximation is poor.

We caution that our R Square differs from the classical R Square (coefficient of determination [30],[31]) although both R Square have an identical formula. In our case, R Square is measured on validation points, not on the modeling points.

The evaluation of R Square is also independent of the types of metamodels.

2) Relative Average Absolute Error (RAAE) [5]

$$RAAE = \frac{\sum_{i=1}^{m}\left|f(\boldsymbol{x_i}) - \hat{f}(\boldsymbol{x_i})\right|}{m * STD} \quad (11)$$

where *STD* stands for standard deviation, $STD = \sqrt{\frac{\sum_{i=1}^{m}[f(x_i) - \bar{f}(x)]^2}{m}}$.

Like R square, this metric shows the overall accuracy of an approximation model. In general, the closer the value of RAAE approaches zero, the more accurate is the approximation model. Similar to the discussion for R square, one can use this metric to find if a model is accurate as compared to its variability.

The caveat is when the function is almost a constant:

$$RAAE = \frac{\sum_{i=1}^{m}\left|f(\boldsymbol{x}_i) - \hat{f}(\boldsymbol{x}_i)\right|}{m * STD} = \frac{\sum_{i=1}^{m}\left|f(\boldsymbol{x}_i) - \hat{f}(\boldsymbol{x}_i)\right|}{\sqrt{m * \sum_{i=1}^{m}\left[f(\boldsymbol{x}_i) - \bar{f}(\boldsymbol{x})\right]^2}} = \frac{1}{\sqrt{m}} lim_{\substack{f(x_i)\to\bar{f}(x) \\ \hat{f}(x_i)\to f(x_i)}} \frac{\sum_{i=1}^{m}|f(\boldsymbol{x}_i) - \hat{f}(\boldsymbol{x}_i)|}{\sqrt{\sum_{i=1}^{m}[f(\boldsymbol{x}_i) - \bar{f}(\boldsymbol{x})]^2}} = \frac{1}{\sqrt{m}} \quad (12)$$

In this case, RAAE value is not zero but approaches to $\frac{1}{\sqrt{m}}$. Therefore, RAAE bears similar disadvantage as R Square when the output is or close to be a constant.

3) Relative Maximum Absolute Error (RMAE) [5]:

$$RMAE = \frac{\max\left(\left|f(\boldsymbol{x}_1) - \hat{f}(\boldsymbol{x}_1)\right|, \left|f(\boldsymbol{x}_2) - \hat{f}(\boldsymbol{x}_2)\right| ,\cdots, \left|f(\boldsymbol{x}_m) - \hat{f}(\boldsymbol{x}_m)\right|\right)}{STD} \quad (13)$$

This is a local metric. A RMAE describes error in a sub-region of the design space. Therefore, a small value of RMAE is preferred. Similarly STD affects RMAE.

The above two subsections defines two sets of performance metrics.

Function-value-scaled set (3)-(5) explains the departure of the metamodel from the underlying function with respect to the function value. Function-variability-scaled set (11)-(13) interprets the modeling error with respect to the function variability. Both sets of performance metrics relate to different characteristics of the underlying function. Each set of performance metrics explains the accuracy of models from different perspectives.

Therefore, these performance metrics work together to reflect the overall goodness of metamodels. The judgment of goodness of a metamodel is related to the characteristics of the underlying function. Practitioners need to carefully examine both sets of metrics and make the judgment from all metrics rather than from one or any arbitrary choice of a subset from the above metrics. For practical algorithm implementation, this work employs MARE and RAAE from each group as convergence criteria for metamodeling.

We set MARE as 0.1 and RAAE as 0.3; either one criterion is met, the modeling process stops. The metamodel is then evaluated against other performance metrics to examine the local performance of the metamodel.

V. Case Studies

This section first introduces the power system of interest, and then describes three different practical operating scenarios to be modeled, and at last the gained understandings of power system and its transfer capability through metamodeling and validation.

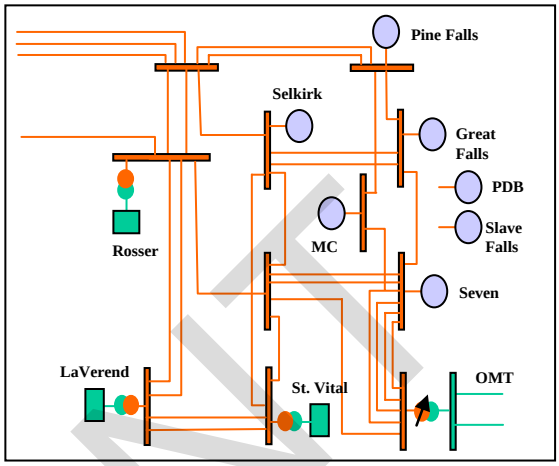

Fig. 3. A single-line diagram of the power system in Winnipeg River area

V.1. Power Grid Description

Fig. 3 shows a single line diagram of the Winnipeg River area system and Manitoba-Ontario interconnections. The 115kV transmission system interconnects the Winnipeg River generating plants, Selkirk generating station, Ontario-Manitoba Tie (OMT), and the major 230kV transmission grid surrounding the City of Winnipeg. There are totally six hydraulic generating plants on the Winnipeg River. Four plants, Seven Sisters (6 generators), Great Falls (6 generators), McArthur Falls (8 generators), and Pine Falls (6 generators) are connected through the 115kV transmission system. The other two plants, Pointe du Bois (PDB) (16 generators) and Slave Falls (8 generators), feed radially into the City of Winnipeg 66kV system. Selkirk generating station is a gas fired thermal plant located near the City of Winnipeg and connected to the 115kV transmission system. The Ontario-Manitoba interconnection consists of two 230kV tie lines from Manitoba to northwestern Ontario. The interface is controlled by the 115kV phase shifting and 115/230kV voltage regulating transformers at Whiteshell station near the Manitoba-Ontario border. Generation levels of the hydraulic plants on the Winnipeg River are a function of river system management and economic operation of the plants. The total generation levels can vary significantly from a maximum of 593 MW to minimum of 298 MW depending on the river flow. The Selkirk generating plant has two units of 65 MW each and is operated when required to regulate the system reliability. It is from the operating experience that the Selkirk generation has a unique impact on the system performance; it will be

interesting therefore to study this impact on the transfer capability of the interconnection. This information will be useful in coordinating generation operations in the concerned areas.

The case studies are for the winter load with all the transmission lines in service. The hydraulic generation levels on Winnipeg River are obtained for each generator in each plant. Temperature is assumed at a 0°C, therefore, the metamodel will not show the sensitivity to the temperature change for the case studies. This power system simulation proceeds with 50 inputs (i.e., the power output from 50 generators) and one parameter (thermal generators at Selkirk for system impact study). The transfer capability of this simulation-based power system can be abstracted as $f = f(\boldsymbol{x}, \rho)$. The input $\boldsymbol{x}$ determines a specific operating scenario, representing the input generators and the parameter ρ denoting the status of the generators at Selkirk. In this study, the transfer capability, f, is defined as the maximum power that can be transferred from Manitoba to Ontario through OMT without violating numerous contingency requirements. It takes about thirteen minutes on a desktop computer (Pentium 4 CPU 2.53 GHz) to evaluate one simulation. Even a huge number of grid points cannot sufficiently cover the entire 50-dimensional input variable space. Scattered outcomes of sporadic simulations do not provide a global understanding of the functional relationship between the transfer capability (f) and generation patterns ($\boldsymbol{x}, \rho$). Three case studies using RBF-HDMR are presented below.

V.2. Tree Model Cases

Three cases are modeled, which include the cases that no Selkirk generators are online ($\rho = 0$), one Selkirk generator with 65 MW is online ($\rho = 1$), and two Selkirk generators with 130 MW are online ($\rho = 2$), respectively. The two sets of performance metrics proposed in Section 4 are used to validate metamodels. In order to observe the changes of these performance metrics, five batches of 100 random test points (non-modeling points) are sequentially and accumulatively used to evaluate the metamodels against the performance metrics until all total 500 test points are used. The values of these performance metrics show the prediction capability of the RBF-HDMR on new input points.

Case 1 No Selkirk Generators on Line ($\rho = 0$)

This metamodel has been constructed by 315 expensive simulation points. Table I lists the performance metric values of accumulated samples of five batches. It shows that the mean absolute relative error (MARE) is less than 7%. The maximum absolute relative error (MxARE) in 500 validation points is 20.23%. The medium absolute error (MdARE) is less that 6%. The values of function-value-scaled performance metrics indicate that the resultant RBF-HDMR metamodel is satisfactory. In the function-variability-scaled set, R Square swings around zero, which indicates the metamodel may not be a good approximation or system output approaches a constant. Such situation warrants the examination of other performance metrics. The Relative Average Absolute Error (RAAE) stays at 0.83, which indicates that the output approaches to a constant. Also the Relative Maximum Absolute Error (RMAE) vibrates at 2.5. These numbers indicate that the metamodel is rather good. If one judges this resultant metamodel only from the R square value, (s)he may misjudge the quality of the metamodel.

TABLE I
PERFORMANCE METRIC VALUES OF CASE 1

Performance metric		*Validation Sample Size*				
		100	200	300	400	500
Value-scaled Set	MARE (%)	6.27	6.72	6.56	6.61	6.57
	MxARE (%)	20.23	20.23	20.23	20.23	20.23
	MdARE (%)	4.89	5.63	5.53	5.64	5.64
Variability-scaled Set	RSquare	0.02	0.00	-0.01	-0.02	0.01
	RAAE	0.79	0.83	0.83	0.83	0.83
	RMAE	2.50	2.48	2.52	2.75	2.75

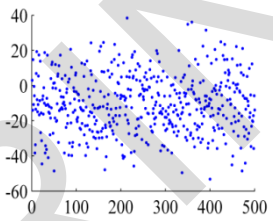

(a) Error Distribution (vertical axis in MW)

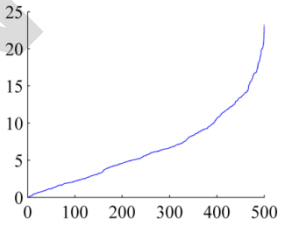

(b) Sorted absolute relative error in percentage

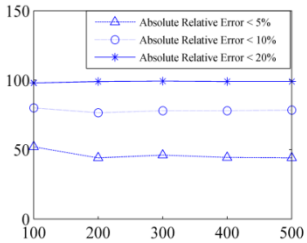

(c) Percentage of absolute relative error less than specific percentiles

Figs. 4. Error plots for Case 1 (with 500 samples)

Fig. 4(a) shows the error distribution of 500 randomly sampled points. In Fig. 4(a), the horizontal coordinate provides the order of the sampled points, and the vertical coordinate represents the errors. The mean of the errors is approximate 10 mega watts (MW), which equals to the predetermined increments of power transfer for OMT.

This error means that the power transfer capability as the function output is discretely simulated at 10 MW increments and thus the mean error is expected to be 10 mega watts.

Fig. 4(b) sorts absolute relative errors of 500 test samples. It demonstrates that the 80% test samples have relative errors of less than 10%. Fig. 4(c) displays the percentage changes of the absolute relative error less than the specific percentiles 5%, 10% and 20%, respectively.

In Fig. 4(c), the horizontal coordinates denotes the number of accumulated samples of five batches and the vertical coordinate represents the percentages. It can be seen that almost 100% sample points have less than 20% relative errors, and about 42% sample points have less than 5%. The percentage of all specified percentiles becomes stable as the test sample size increases.

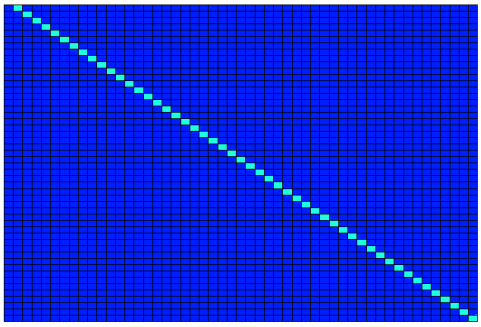

Fig. 5. Structure matrix for Case 1

Fig. 5 shows the structure matrix of this case. A structure matrix is an output of the metamodeling process that captures significant terms in the RBF-HDMR expression as defined in (1). Any bright dot in the structure shows a variable correlation. Fig. 5 shows a 50x50 matrix with only diagonal terms, which means that the function consists of only the constant term and the first-order terms, and there is no significant correlations between generators. In all first-order terms, some terms are linear, and others are nonlinear. The linearity/non-linearity of each component is stored in the final model. In more detail, the functional form is written as:

$$f(\boldsymbol{x}) \cong f_0 + \\ + \sum_{i=1\cdots8,20,24,27\cdots50} \sum_{k=1}^{m_i} \alpha_{i_k} \left| \begin{matrix} (x_i, \boldsymbol{x}_0^i) \\ -(x_{i_k}, \boldsymbol{x}_0^i) \end{matrix} \right| + \\ + \sum_{i=9,\cdots,19,21,22,23,25,26} \sum_{k=1}^{m_i} \alpha_{i_k} \left| \begin{matrix} (x_i, \boldsymbol{x}_0^i) \\ -(x_{i_k}, \boldsymbol{x}_0^i) \end{matrix} \right| \quad (14)$$

where $f_0 = 264MW$, the coefficients $\boldsymbol{\alpha}_i$ for each input variable x_i in the second term of (14) is zero, which shows both linearity and no contribution to the variation of transfer capability $f(\boldsymbol{x})$. The variation of transfer capability $f(\boldsymbol{x})$ is brought about by the last term. The magnitude of coefficients embodies the sensitivity of corresponding generators to the transfer capability. Due to high-dimensionality and limited space, we choose to plot the metamodel curves of only three generators in Figs. 6. In Figs. 6, the horizontal axis denotes the outputs of a generator and vertical axis represents the transfer capabilities.

The dots display the modeling points. Fig. 6(a) is the plot of the first generator at Great Falls, Fig. 6(b) is the plot of the first generator at Seven Sisters and Fig. 6(c) is the plot of the first generator at Pine Falls. One can see that model interpolates the modelling points. Also the output varies within a small region (between 250-275 MW) with largely flat regions.

Case 2 One Selkirk Generator on Line ($\rho = 1$)

For this case, one Selkirk generator with 65 MW is on line ($\rho = 1$). The resultant metamodel is built by 251 expensive simulation points. Table 2 displays the values of two sets of performance metrics with test samples of various size. The mean absolute relative error (MARE) reaches 0.03%. The maximum absolute relative error ($MxARE$) is 4.9%. The medium absolute relative error (MdARE) is zero.

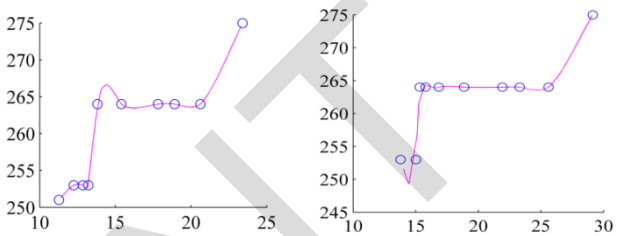

(a) generator at Great Falls (b) generator at Seven Sisters

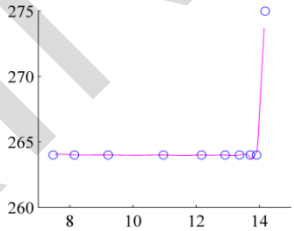

(c) generator at Pine Falls

Figs. 6. Transfer capability impact curves of three generators; *x* axis shows the output from each generator and *y* axis is the power transfer at OMT. Unit: MW

The values of the function-value-scaled performance metrics indicate that the resultant RBF-HDMR accurately predicts the transfer capability. All R Square values are negative and close to zero. This phenomenon indicates that the current metamodel is either not accurate enough to approximate the simulation system, or the simulation function values are close to a constant. The final judgment needs to be supported by other performance metrics. Relative average absolute error (RAAE) has small values as the test sample size increases. Relative Maximum Absolute Error (RMAE) increases as the standard deviation decreases. The relative error of all test samples is less than 5%. All these performance metrics except R Square support that the transfer capability of the power system is a constant (300 MW) and the final RBF-HDMR model is a good approximation of the transfer capability under this operating scenario.

Among additional 500 random samples, the predicated value equals to the actual value at 482 points; the four points have -1 (MW) errors; the thirteen points have -2 (MW) errors; and only one has -14 (MW) error. For this case, since the transfer capability is a constant 300 MW, the influence of the 10 MW increment does not exist.

The 13 smaller errors may be due to the control dead-band (acceptable deviation) of the phase shifting transformers. Other is believed to be an outlier. For clarity, Fig. 7 shows the error distribution. It shows that the errors distribute close to zero.

TABLE II
PERFORMANCE METRIC VALUES OF CASE 2

Performance metric		*Validation Sample Size*				
		100	200	300	400	500
Value-scaled Set	MARE (%)	0.08	0.05	0.04	0.03	0.03
	MxARE (%)	4.90	4.90	4.90	4.90	4.90
	MdARE (%)	0	0	0	0	0
Variability-scaled Set	R Square	-0.02	-0.02	-0.02	-0.01	-0.01
	RAAE	0.16	0.14	0.14	0.13	0.13
	RMAE	9.7	13.3	15.9	18.1	19.8

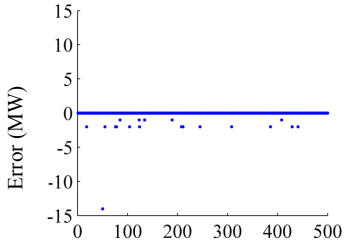

Fig. 7. Error distribution of Case 2 (with 500 samples)

Fig. 8 plots the statistical data of 500 random samples for this case. The top plot displays the change of the mean of different test sample sizes. It can be seen that the mean approaches the constant 300 MW. The middle plot shows the standard deviation of the samples. The deviation becomes smaller as the sample size increases. The bottom plot explains the variance of this case. The variance becomes smaller as the sample size increases as well.

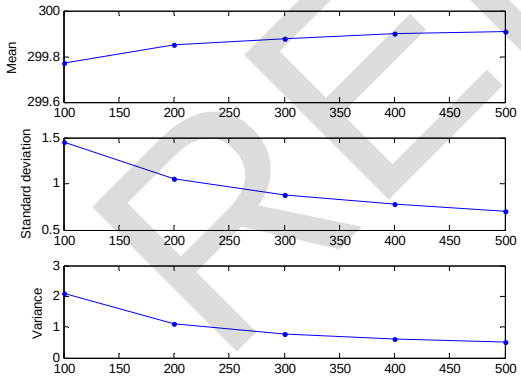

Fig. 8. Statistics of transfer capability for Case 2 (vertical axis unit: MW)

The structure matrix of Case 2 shows a similar structure as that of Case 1, as shown in Fig. 4, which indicates there is no significant correlation between generators. The functional form can be written as:

$$f(\boldsymbol{x}) \cong f_0 + \sum_{i=1}^{50}\sum_{k=1}^{m_i} \alpha_{i_k}\left|\left(x_i, \boldsymbol{x}_0^i\right) - \left(x_{i_k}, \boldsymbol{x}_0^i\right)\right| \qquad (15)$$

where $f_0 = 300MW$, all the coefficients $\boldsymbol{\alpha}_i$ for each input variable x_i are close to be zeroes. All of first-order terms are linear. The linearity/non-linearity of each component can be found in the final model. No generator causes significant changes of the transfer capability. In other words, this indicates that the transfer capability reaches a stable state of 300 MW.

Case 3 Two Selkirk Generators on Line ($\rho = 2$)

In Case 3, two Selkirk generators with 130 MW are on line ($\rho = 2$). The cost of the final metamodel consists of 284 expensive evaluation samples. Table III gives the performance metric values of various test samples. The mean absolute relative error (MARE) is approximate 0.4%. The maximum absolute relative error (MxARE) has 9.04%. The medium absolute relative error (MdARE) is 0.05%. The values of function-value-scaled performance metrics display the accuracy of the final RBF-HDMR prediction. R Square values swings around zero which indicates that the transfer capability is around some certain constant. Relative Average Absolute Error (RAAE) is under 0.4.

TABLE III
PERFORMANCE METRIC VALUES OF CASE 3

Performance metric		*Validation Sample Size*				
		100	200	300	400	500
Value-scaled Set	MARE (%)	0.42	0.39	0.36	0. 35	0. 36
	MxARE (%)	9.04	9.04	9.04	9.04	9.04
	MdARE (%)	0.04	0.05	0.05	0.05	0.05
Variability-scaled Set	R Square	0.09	0.01	-0.03	-0.04	0.01
	RAAE	0.30	0.35	0.38	0.39	0.36
	RMAE	6.06	7.65	8.91	9.53	8.37

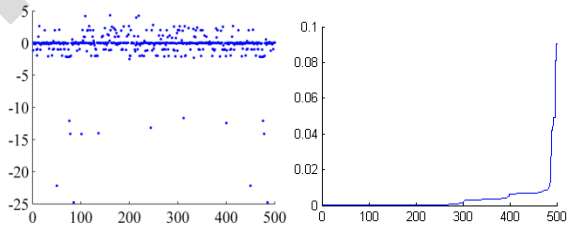

(a) Error distribution (MW) (b) Absolute relative errors

Figs. 9. Values of case 3 (vertical axis unit: MW)

Fig. 9(a) displays the predicted and actual values of 500 random test samples. For clarity, Fig. 9(b) plots the trends of the first 100 of 500 test samples, which shows the final

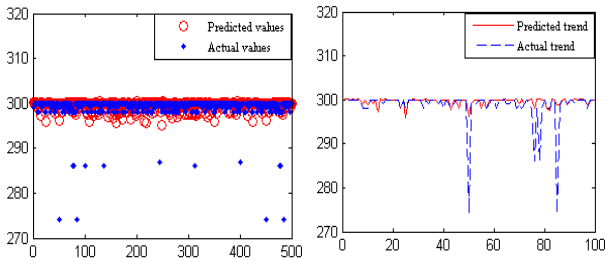

(a) Output values for 500 samples (b) Output for the first 100 test samples

Figs. 10. Errors of Case 3(with 500 samples)

RBF-HDMR captures the overall trends of the model behavior. Fig. 10(a) shows the error distribution. Those errors distribute close to zero except for thirteen points. Some of these errors may be due to the 10 MW simulation increment. In other words, the transfer capability may not be at 300 MW for some generation patterns. Some others may be outliers. Fig. 10(b) shows the absolute relative errors. These relative errors are small except for thirteen points. The outputs are close to a constant, that is, its variance is small. The mean of various sizes of samples is approximate 299 MW. It can be seen that the final RBF-HDMR accurately predicts the outputs of the simulation function except for thirteen points.

The structure matrix is similar to that of Case 1, which still shows no correlation between input generators. The functional form is:

$$f(\boldsymbol{x}) \cong f_0 + \sum_{i=1\cdots 8,10,12,13,19,\cdots,50} \sum_{k=1}^{m_i} \alpha_{i_k} \left| \left(x_{\boldsymbol{i}}, \boldsymbol{x}_0^i\right) - \left(x_{\boldsymbol{i_k}}, \boldsymbol{x}_0^i\right) \right| + \sum_{i=9,11,14,\cdots,18} \sum_{k=1}^{m_i} \alpha_{i_k} \left| \left(x_{\boldsymbol{i}}, \boldsymbol{x}_0^i\right) - \left(x_{\boldsymbol{i_k}}, \boldsymbol{x}_0^i\right) \right| \quad (16)$$

where $f_0 = 300MW$, the coefficient $\boldsymbol{\alpha}_i$ in the second term is a $\mathbf{0}$ vector, and the linearity/nonlinearity of these components can be obtained in the final metamodel. The variation of transfer capability $f(\boldsymbol{x})$ is brought by the last term. The nonlinearity information of the components in the last term can be found in the model. The magnitude of coefficients reflects the sensitivities of generators.

Three generators in Great Falls and two generators in Seven Sisters contributed to variation of transfer capability$f(\boldsymbol{x})$.

V.3. Understanding of Power Grid and Transfer Capability

In Section V.2, three model cases have been developed by RBF-HDMR with satisfactory results. The resultant RBF-HDMRs capture the characteristics of power grid under different state parameter ρ and achieve good accuracy of the transfer capability prediction for Ontario-Manitoba interconnection. Each model finds the functional form of underlying power grid which discloses the relative importance of generators to the power transfer capabilities. As the nonlinearity of underlying power grid changes, the functional forms of the resultant models change, which can be seen from comparison of (14), (15) and (16) (Please refer to Appendix for the exact function form). The modeling cost also varies. As the nonlinear terms increase, the modeling cost increase.

The underlying system model in Case 1 has the most nonlinear terms in (14) and costs 315 simulation points; the model in Case 3 has less nonlinear terms in (16) and costs 284 simulation points; and the linear underlying system model in Case 2 has no nonlinear terms and costs only 251 simulation points. The resultant models show that the thermal generating plant at Selkirk plays an important role in determining the transfer capability over OMT interconnection.

For Case 1 when both generators in Selkirk are off line, the power transfer capability is strongly impacted by the hydraulic generation patterns. This impact is highly nonlinear and exerted mainly by generators in three hydraulic generating plants (Great Falls, Seven Sisters and Pine Falls). With one generator at Selkirk (Case 2) on line, the transfer capability is beyond 300 MW. Any individual generator will not impact the transfer capability at this transfer level.

When two generators at Selkirk are on line (Case 3), the transfer capability of the power grid manifests low-order nonlinearity, which means the stability of transfer capability becomes worse than in Case 2. The transfer capability is mildly impacted by generators from two generating plants (Great Falls and Seven sisters). These observations are supported by the system operating experience from field experts.

In summary, both RBF-HDMR models and experts' operational experience indicate that the Selkirk generation has a unique regulatory impact on the power transfer capability on the Manitoba-Ontario interconnection. It is anticipated that Case 1 with no Selkirk generation and Case 3 with both units on line would display more nonlinear characteristics while Case 2 with one unit on line shows fairly linear characteristics and is the most favorable operating condition.

Based on the observations of the three case studies from modeling standpoint, we can conclude that RBF-HDME models all three cases well.

Among them, Case 2 is modeled the best, Case 3 is ranked second, and Case 1 is third. This conclusion is supported by the performance metrics in Tables I-III. The mean absolute relative error (MARE) values are ranked by order of Case 2, Case 3 and Case 1. The relative average absolute error (RAAE) values are ranked in the same order as MARE, which indicates the consistency. All R Square values of three cases are close to 0, which is due to the fact that their outputs all approach to a constant. Both Cases 2 and 3 approach 300 MW and the error distribution of Case 3 is more scattered than that of Case 2. The mean of Case 1 approaches a constant of 264 MW and shows high nonlinearity. In Case 1, error distribution is much more scattered than those for both Case 2 and Case 3. These results also show that the proposed performance metric sets overcome the deficiency of a single metric to avoid potential misjudgment.

Compared with traditional metamodeling methods by using a full polynomial function of five variables [16], our experience is that RBF-HDMR model has obvious advantages in efficiency and accuracy for HEB problems.

The computational cost of the five-variable cases is, on average, about two times higher than that for 50 variables using RBF-HDMR.

Attempts have been made to build a metamodel using other metamodeling techniques such as Kriging and RBF.

However due to the high dimensionality and cost associated, the attempts have not been successful.

VI. Summary

The contributions of this paper are summarized as below.

First, the work applies the RBF-HDMR metamodeling technique to model a 50-variable large-scale system, i.e., the transfer capability of the Manitoba-Ontario Interconnection under various operating conditions. To the authors' best knowledge, such high dimensionality is the largest scale of a real-world problem that metamodeling has ever been successfully applied to. The results demonstrate that RBF-HDMR model can capture characteristics of the studied power system and achieve a good prediction of transfer capability with a maximum of only 315 expensive simulations.

Second, the metamodeling strategy is able to model complicated power systems with many contingency and system reliability checks. This capability complements optimal power flow (OPF) analysis and is not provided by commercial power system analysis tools.

The result of the work enhances the understanding of the performance of the Manitoba-Ontario interconnected power system. The developed metamodels provide useful tools for power system planning.

Thirdly, the works identifies the deficiency of some commonly used performance metrics and proposes two complementary sets of modified metrics for metamodel validation.

The deficiency, which is caused mostly by the division of zeros due to constant function values, is the first time being reported. The risk of misjudgment using such metrics for metamodel validation has been demonstrated through the case studies of the power system.

The two sets of modified performance metrics address the accuracy of the metamodel from both function value and variation perspectives, and therefore offering a comprehensive set of metrics for metamodel validation in general.

Appendix

RBF model

A general radial basis functions (RBF) model [5, 6] is shown as:

$$\hat{f}(\boldsymbol{x}) = \sum_{i=1}^{n} \beta_i \varphi(|\boldsymbol{x} - \boldsymbol{x}_i|) \tag{A.1}$$

where β_i is the coefficient of the expression and $\boldsymbol{x}_i$ are the sampled points of input variables or the centers of RBF approximation. $\varphi(.)$ is a distance function or the radial basis function. $|.|$ denotes a *p*-norm distance. A RBF is a real-valued function whose value depends only on the distance from center points $\boldsymbol{x}_i$.

It employs linear combinations of a radically symmetric function based on the distance to approximate underlying functions. Its advantages include: the number of sampled points for constructing approximation can be small and the approximations are good fits to arbitrary contours of response functions [6]. Consequently, RBF is a popular model for multivariate data interpolation and function approximations.

The key of RBF approach is to choose a *p*-norm and a radial basis function $\phi(\cdot)$, both of which have multiple formats. One of the goals for choosing a format is to make the distance matrix ($A_{ij} = \varphi(|\boldsymbol{x}_i - \boldsymbol{x}_j|)$, for $1 \le i, j \le n$, n is the number of sample points) non-singular.

The singularity of the distance matrix relates to the distribution of the sample points. It can be seen that there are many works on choosing a *p*-norm and a radial basis function $\varphi(.)$ to avoid the singularity of the distance matrix [32].

This research uses a sum of thin plate spline (the first term) plus a linear polynomial $P(\boldsymbol{x})$ (the second term):

$$\begin{aligned} &\hat{f}(\boldsymbol{x}) = \sum_{i=1}^{n} \beta_i |\boldsymbol{x} - \boldsymbol{x}_i|^2 log|\boldsymbol{x} - \boldsymbol{x}_i| + P(\boldsymbol{x}), \\ &\sum_{i=1}^{n} \beta_i \boldsymbol{p}(\boldsymbol{x}) = \boldsymbol{0}, \qquad P(\boldsymbol{x}) = \boldsymbol{p}\boldsymbol{\alpha} = \\ &= [p_1, p_2, \cdots, p_q][\alpha_1, \alpha_2, \cdots, \alpha_q]^T \end{aligned} \tag{A.2}$$

where $\boldsymbol{x}_i$ are the vectors of evaluated *n* sample points; the coefficients $\boldsymbol{\beta} = [\beta_1, \beta_2, \cdots, \beta_n]$ and α are parameters to be found. $P(\boldsymbol{x})$ is a polynomial function, where $\boldsymbol{p}$ consists of a vector of basis of polynomials. In this work, $\boldsymbol{p}$ is chosen to be $(1, x_1, \cdots, x_d)$ including only linear variable terms and therefore q=d+1;

The side condition $\sum_{i=1}^{n} \beta_i \boldsymbol{p}(\boldsymbol{x}) = 0$ is imposed on the coefficients $\boldsymbol{\beta}$ to improve an under-determined system, that is, the singularity of distance matrix $\boldsymbol{A}$ [32].

To calculate the coefficients $\boldsymbol{\beta}$ and $\boldsymbol{\alpha}$, (A.2) may be written in the matrix form as:

$$\begin{bmatrix} A & \tilde{P} \\ \tilde{P}^T & 0 \end{bmatrix} \begin{bmatrix} \beta \\ \alpha \end{bmatrix} = \begin{bmatrix} f \\ 0 \end{bmatrix} \tag{A.3}$$

where:

$$\begin{aligned} A_{ij} &= |\boldsymbol{x}_i - \boldsymbol{x}_j|^2 log|\boldsymbol{x}_i - \boldsymbol{x}_j|, \ \ i, j = 1, \cdots, n, \\ \tilde{P}_{ij} &= p_j(\boldsymbol{x}_i), \qquad i = 1, \cdots, n; \ \ j = 1, \cdots, (d+1) \end{aligned}$$

and $\boldsymbol{x}_i$ and $\boldsymbol{x}_j$ are the vectors of evaluated *n* sample points.

The theory guarantees the existence of a unique vector $\boldsymbol{\beta}$ and a unique polynomial $P(\boldsymbol{x})$ satisfying (A.2) [32].

Acknowledgements

Financial supports from Manitoba Hydro and Natural Science and Engineering Research Council (NSERC) of Canada are gratefully acknowledged.

References

[1] R. H. Myers, and D. Montgomery, *Response Surface Methodology: Process and Product Optimization Using Designed Experiments*, John Wiley and Sons, Inc., Toronto, 1995.

[2] G. E. P. Box, J. S. Hunter, and W. G. Hunter, *Statistics for Experimenters: Design, Innovation, and Discovery* John Wiley & Sons, Inc., Hoboken, New Jersey, 2005.

[3] J. Sacks, W. J. Welch, T. J. Mitchell, and H. P. Wynn, "Design and Analysis of Computer Experiments," *Statistical Science*, 4(4), pp. 409-435, 1989.

[4] T. W. Simpson, T. M. Mauery, J. J. Korte, and F. Mistree, "Kriging Metamodels for Global Approximation in Simulation-Based Multidisciplinary Design Optimization," *AIAA Journal*, 39(12), pp. 2233-2241, 2001.

[5] R. Jin, W. Chen, and T. W. Simpson, "Comparative Studies of Metamodeling Techniques under Multiple Modeling Criteria," *Structural and Multidisciplinary Optimization*, 23(1), pp. 1-13, 2001.

[6] V. C. P. Chen, K.-L. Tsui, R. R. Barton, and M., Meckesheimer, "A Review on Design, Modeling and Applications of Computer Experiments," *IIE Transactions*, 38, pp. 273-291, 2006.

[7] S. M. Clarke, J. H. Griebsch, and T. W. Simpson, "Analysis of Support Vector Regression for Approximation of Complex Engineering Analyses," *Transactions of ASME, Journal of Mechanical Design*, 127(6), pp. 1077-1087, 2005.

[8] A. A. Giunta, and L. T. Watson, "A Comparison of Approximation Modeling Techniques: Polynomial Versus Interpolating Models," *Proceedings of the 7th AIAA/USAF/NASA/ISSMO Symposium on Multidisciplinary Analysis & Optimization*, American Institute of Aeronautics and Astronautics, Inc., St. Louis, MO, Vol. 1, pp. 392-401, 1998.

[9] F. A. C. Viana, R. T. Haftka, and V. J. Steffen, "Multiple Surrogates: How Cross-Validation Errors Can Help Us to Obtain the Best Predictor," *Structural and Multidisciplinary Optimization*, 39(4), pp. 439-457, 2009.

[10] E. Acar, and M. Rais-Rohani, "Ensemble of Metamodels with Optimized Weight Factors," *Structural and Multidisciplinary Optimization*, 37, pp. 279-294, 2009.

[11] T. Goel, R. T. Haftka, W. Shyy, and N. V. Queipo, "Ensemble of Surrogates," *Structural and Multidisciplinary Optimization*, 33, pp. 199-216, 2007.

[12] R. C. Kuczera, and Z. P. Mourelatos, "On Estimating the Reliability of Multiple Failure Region Problems Using Approximate Metamodels," *Transactions of the ASME, Journal of Mechanical Design*, 131(12), 2009.

[13] R. J. Yang, N. Wang, C. H. Tho, and J. P. Bobineau, "Metamodeling Development for Vehicle Frontal Impact Simulation," *Transactions of the ASME, Journal of Mechanical Design*, 127, pp. 1014-1020, 2005.

[14] D. W. Apley, J. Liu, and W. Chen, "Understanding the Effects of Model Uncertainty in Robust Design with Computer Experiments," *Transactions of the ASME, Journal of Mechanical Design*, 128, pp. 945-958, 2006.

[15] C. A. Georgopoulou, and K. C. Giannakoglou, "Metamodel-Assisted Evolutionary Algorithms for the Unit Commitment Problem with Probabilistic Outages," *Applied Energy*, 87(2010), pp. 1782-1792.

[16] S. Shan, W. Zhang, M. Cavers, and G. G. Wang, "Application of Metamodeling Techniques to Power Transfer Capability Analysis of Manitoba-Ontario Electrical Interconnections," *Proceedings of The Canadian Society for Mechanical Engineering Forum 2010*, Victoria, British Columbia, Canada, June 7-9, 2010.

[17] A. AL-Masri, M. Z. A. Ab Kadir, H. Hizam, N. Mariun, A. Khairuddin, J. Jasni, "Enhancement in Static Security Assessment for a Power System Using an Optimal Artificial Neural Network," *International Review of Electrical Engineering (IREE)*, Vol. 5, n. 3, pp. 1095-1102.

[18] *S. Kaewarsa, and K. Attakitmongcol,* "Classification of Power Quality Disturbances by Using DOS-Transform and Support Vector Machines," *International Review of Electrical Engineering (IREE)*, Vol. 5, n. 5, pp. 2177-2185.

[19] S. Shan, and G. G. Wang, "Survey of Modeling and Optimization Strategies to Solve High-dimensional Design Problems with Computationally-Expensive Black-box Functions," *Structural and Multidisciplinary Optimization*, 41(2(2010)), pp. 219-241.

[20] S. Shan, and G. G. Wang, "Metamodeling for High-dimensional Simulation-Based Design Problems," *Transactions of the ASME, Journal of Mechanical Design*, 132(5), pp. 051009-1-051009-11, 2010.

[21] S. Shan, and G. G. Wang, "Turning Black-box into White Functions," *Transactions of the ASME, Journal of Mechanical Design,* Vol.133, Iss.3, DOI: 10.1115/1.4002978, Feb. 2011.

[22] I. M. Sobol', "Sensitivity Estimates for Nonlinear Mathematical Models," Mathematical Modeling & Computational Experiment, 1(4), pp. 407-414, 1993.

[23] H. Rabitz, H. and Ö. F. Al1s, "General Foundations of High-Dimensional Model Representations," Journal of Mathematical Chemistry, (25), pp. 197-233, 1999.

[24] Y. Lin, J. K. Allen, and F. Mistree, "Metamodel Validation with Deterministic Computer Experiments," *9th AIAA/ISSMO Symposium on Multidisciplinary Analysis and Optimization*, 4-6 September 2002, Atlanta, Georgia, AIAA 2002-5425, 2002.

[25] M. Meckesheimer, and A. J. Booker, "Computationally Inexpensive Metamodel Assessment Strategies," *AIAA Journal*, 40(10), pp. 2053-2060, 2002.

[26] J. P. C. Kleijnen, and R. G. Sargent, "A Methodology for Fitting and Validating Metamodels in Simulation," *European Journal of Operational Research*, 120(2000), pp. 14-29, 2000.

[27] D. Gorissen, I. Couckuyt, E. Laermans, and T. Dhaene, "Multiobjective Global Surrogate Modeling, Dealing with the 5-Percent Problem," *Engineering with Computers*, 26, pp. 81-98, 2010.

[28] Mojgan Hojabri, Hashim Hizam, Norman Mariun, Senan Mahmod Abdullah, Edris Pouresmaeil, "Available Transfer Capability for Power System Planning Using Krylov-Algebraic Method," *International Review of Electrical Engineering (IREE)*, Vol. 5, n. 5, pp. 2251-2162.

[29] Power technologies, I., *Iplan Program Manual*, 2000.

[30] J. P. C. Kleijnen, and D. Deflandre, "Validation of Regression Metamodels in Simulation: Bootstrap Approach," *European Journal of Operational Research*, 170(2006), pp. 120-131, 2006.

[31] M. I. R. d. Santos, and A. c. M. O. P. Nova, "Statistical Fitting and Validation of Non-Linear Simulation Metamodels: A Case Study," *European Journal of Operational Research*, 171 (2006), pp. 53-63, 2006.

[32] B. J. C. Baxter, *The Interpolation Theory of Radial Basis Functions*, Trinity College, Cambridge University, Ph. D. Thesis, 1992.

Authors' information

Songqing Shan's research interests include simulation modeling, design and analysis of computer experiments, metamodeling techniques, computational design and optimization, reliability modeling, rough set application and mechanical system design methodology.

Wenjie Zhang received B.Sc. and M. Sc. degrees in electrical engineering from Huazhong University of Science and Technology and Taiyuan University of Science and Technology in 1982 and 1985, respectively, and Ph.D. degree from The University of British Columbia in 1993. He is a Principal Network Studies Engineer in System Performance

Department at Manitoba Hydro responsible for developing operating guides and procedures for the operations of Manitoba transmission systems and Manitoba-USA and Manitoba-Ontario interconnections. His research interest is in the area of power system control and optimization. Wenjie is a member of PES and a registered professional engineer in the province of Manitoba.

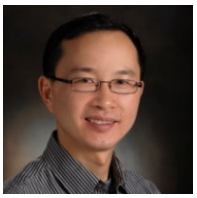

G. Gary Wang received Ph.D. from University of Victoria, Canada, in 1999. He is currently a full professor at Simon Fraser University, BC, Canada. Dr. Wang is active in research on design optimization and advanced manufacturing. He has published close to 50 journal papers in related areas. Dr. Wang is the recipient of the 2005 National I. W. Smith award for creative engineering from Canadian Society of Mechanical Engineering (CSME), as well as the 2007 Rh Award from UM for outstanding research contribution in the Applied Science category. Dr. Wang is currently serving as an associate editor for Journal of Engineering optimization, geographically covering North America. He is also the conference chair for 2012 Design Automation Conference, a sub-conference in the premier ASME International Design Engineering Technical Conference (IDETC).

International Review on Modelling and Simulations
(IREMOS)

(continued from outside front cover)

(continued on outside back cover)

Abstracting and Indexing Information:

Academic Search Complete - EBSCO Information Services
Cambridge Scientific Abstracts - CSA/CIG
Elsevier Bibliographic Database SCOPUS
Index Copernicus (Journal Master List): ***Impact Factor 6.55***

Autorizzazione del Tribunale di Napoli n. 78 del 1/10/2008

(continued from inside back cover)

(continued on Part B)

This volume cannot be sold separately by Part B

1974-9821(201204)5:2;1-T